Sequence-specific binding of counterions to *B*-DNA

Vladimir P. Denisov and Bertil Halle*

Physical Chemistry 2, Lund University, P.O. Box 124, SE-221 00 Lund, Sweden

Edited by Richard E. Dickerson, University of California, Los Angeles, CA, and approved November 23, 1999 (received for review September 14, 1999)

Recent studies by x-ray crystallography, NMR, and molecular simulations have suggested that monovalent counterions can penetrate deeply into the minor groove of *B* form DNA. Such groove-bound ions potentially could play an important role in AT-tract bending and groove narrowing, thereby modulating DNA function *in vivo*. To address this issue, we report here ^{23}Na magnetic relaxation dispersion measurements on oligonucleotides, including difference experiments with the groove-binding drug netropsin. The exquisite sensitivity of this method to ions in long-lived and intimate association with DNA allows us to detect sequence-specific sodium ion binding in the minor groove AT tract of three *B*-DNA dodecamers. The sodium ion occupancy is only a few percent, however, and therefore is not likely to contribute importantly to the ensemble of *B*-DNA structures. We also report results of ion competition experiments, indicating that potassium, rubidium, and cesium ions bind to the minor groove with similarly weak affinity as sodium ions, whereas ammonium ion binding is somewhat stronger. The present findings are discussed in the light of previous NMR and diffraction studies of sequence-specific counterion binding to DNA.

By virtue of its highly charged phosphate backbone, double-helical DNA is engaged in strong electrostatic interactions. The neutralizing charge is provided by mobile counterions in the surrounding aqueous medium or, in protein–DNA complexes, by cationic amino acid side chains. Whereas the diffuse counterion atmosphere around DNA has been studied thoroughly, less is known about sequence-dependent association of monovalent ions to *B*-form DNA and its possible implications for DNA structure and function (1, 2).

Being isoelectronic, Na^+ and H_2O are not easily distinguishable by x-ray diffraction, and with few exceptions (3, 4), the sodium counterions in nucleic acid crystals have escaped detection. Nevertheless, it has been argued on the basis of indirect crystallographic evidence that the primary solvation sites of the so-called "spine of hydration" in the narrow minor groove of the $[d(CGCGAATTCGCG)]_2$ duplex (hereafter referred to as A_2T_2) are not exclusively occupied by water molecules but are partly substituted by Na^+ ions (5, 6). However, a subsequent atomic-resolution (1.1 Å) study of the same duplex (but with a 4-fold higher Mg^{2+}/Na^+ ratio in the crystallizing solution) did not find any evidence, direct or indirect, for the presence of Na^+ ions in the minor groove (7). Another study (8) found that the Mg^{2+} salt of the cross-linked A_2T_2 duplex (with virtually no monovalent ions present in the crystal) has essentially the same structure (at 1.43-Å resolution) as the Na^+ salt of the native duplex (at 1.9 Å) (9). This indicates that the crystal structure of the A_2T_2 duplex is not affected significantly by localized binding of Na^+ ions (whether they are present in the minor groove or not). The authors of this recent work (8) challenged the earlier arguments in favor of groove-bound Na^+ ions (5) and also questioned the validity of the procedure used to infer, from crystallographic data, partial occupancy of K^+ ions at several primary solvation sites in the minor groove of the K^+ salt of the A_2T_2 duplex (10). Even if one admits that there exists no unambiguous crystallographic evidence for partial Na^+ or K^+ substitution for water molecules in the minor-groove spine of hydration, this does not necessarily mean that such ions are not there. X-ray crystallography simply cannot detect them (at present). Conditions are more favorable for the heavier alkali metal ions. A Rb^+ ion thus has been localized (with about 50% occupancy) at the central ApT step of the A_2T_2 duplex (11). This appears to be the strongest crystallographic case for monovalent ion penetration of the minor groove. As regards Cs^+, the situation is less clear. Whereas fiber diffraction data from phage T2 CsDNA were modeled successfully with fully occupied Cs^+ sites in 6 of 10 base-stacking types (12), a single-crystal diffraction study of the Cs^+ salt of d(CGCGAATTCGCG) appears to rule out Cs^+ penetration of the minor groove (11).

Even if the duplex morphology can be shown to be nearly the same in solution as in the crystal, the probability that a nominal solvation site in the minor groove is occupied by a certain type of ion may be quite different under the two conditions. In particular, the cryogenic temperatures used in all recent crystallographic work may drastically shift the enthalpy–entropy balance of ion–water substitution. The low water content and crystal-packing effects are also of concern in this regard. Solution studies therefore are needed to settle the issue of sequence-specific counterion binding to DNA under physiological conditions. Molecular dynamics (MD) simulations, in principle, can provide this type of information. A recent MD study thus showed that a Na^+ ion resides (with >50% occupancy) at the central ApT step of the A_2T_2 duplex (13, 14), a location that is known to have a uniquely low electrostatic potential (13, 15). Another MD study found Na^+ ions (with 5–40% occupancy) at primary solvation sites throughout the minor and major grooves of the same duplex (16). Even Cl^- ions were found to substitute for primary hydration waters in the minor groove (16). At present, however, MD results bearing on the issue of ion penetration of the minor groove must be viewed with caution. Depending on the force field used, duplex morphologies resembling either the *A* form or the *B* form are obtained (17). Furthermore, none of the most widely used force fields directly incorporate polarization effects, which may be crucial for the energetics of ion–water substitution in the minor groove.

Evidence for ion penetration of the minor groove recently has been reported for *B*-DNA oligonucleotides in solution. Using ^{1}H nuclear Overhauser effect spectroscopy (NOESY), Hud *et al.* (18) demonstrated partial occupancy of NH_4^+ ions in several primary solvation sites of the minor groove in three *B*-DNA duplexes containing extended AT tracts. The observation of NOESY cross-peaks with $^{15}NH_4^+$ in both GCA_4T_4GC and CGT_4A_4CG demonstrated that an ApT step is not needed for ion intrusion into the minor groove (18). The same group previously demonstrated that Mn^{2+} ions have access to the floor of the minor groove AT tracts of these two dodecamers (19).

Among the alkali metals, ^{23}Na is best suited for NMR quadrupole relaxation studies, and a large number of such studies have been carried out on DNA (20–25). A general conclusion

This paper was submitted directly (Track II) to the PNAS office.

Abbreviations: A_2T_2, d(CGCGAATTCGCG); MD, molecular dynamics; MRD, magnetic relaxation dispersion; NOESY, nuclear Overhauser effect spectroscopy; QCC, quadrupole coupling constant; SDF, spectral density function.

*To whom reprint requests should be addressed. E-mail: bertil.halle@fkem2.lth.se.

The publication costs of this article were defrayed in part by page charge payment. This article must therefore be hereby marked "*advertisement*" in accordance with 18 U.S.C. §1734 solely to indicate this fact.

from these studies is that monovalent counterion binding to DNA is loose and delocalized, without any dehydration or sequence-specific features (25). It can be argued, however, that previous ^{23}Na NMR experiments were not optimally designed to test for sequence-specific Na^+ binding in the minor groove of DNA. In the present work, we therefore introduce several novel strategies. First, this is a magnetic relaxation dispersion (MRD) study, where the ^{23}Na relaxation rate is measured over nearly two decades of resonance frequency (26). Most previous ^{23}Na relaxation studies have been restricted to one or a few frequencies, thus precluding an unambiguous separation of static factors (ion occupancy, quadrupole coupling) and dynamic factors (motional correlation times). Second, we compare ^{23}Na MRD data from three dodecamers with different nucleotide sequences. In contrast, nearly all previous ^{23}Na NMR studies have involved polymeric DNA of general base sequence. Third, we use the minor groove-binding drug netropsin to selectively displace any intruding counterions. We previously have used this approach in ^{2}H and ^{17}O MRD studies of DNA hydration (27, 28). We also report ^{23}Na relaxation data recorded in the presence of the competing counterions K^+, Rb^+, Cs^+, and NH_4^+.

Materials and Methods

Sample Preparation. DNA dodecamers with the sequences CGCGAATTCGCG (abbreviated A_2T_2), CGAAAATTTTCG (A_4T_4), and CGCTCTAGAGCG (TA) were synthesized and purified as described (28) with the fraction full-length oligomer estimated by HPLC to 80–90%. The solvent was either D_2O with 99.9 atom% ^{2}H (for A_2T_2) or HDO with 51.8 atom% ^{2}H (for A_4T_4 and TA). Solution pH (not corrected for isotope effects) was adjusted to 7.00 ± 0.02. No buffers were added. All samples were annealed by slow (30–60 min) cooling from 75°C to room temperature. Duplex DNA concentrations were 8.2 mM (A_2T_2), 8.6 mM (A_4T_4), and 7.8 mM (TA). Na^+ concentrations, estimated from the ^{23}Na resonance at 79.3 MHz by comparing the peak area with that from a $NaClO_4$ solution in acetone (chemical shift difference 7.25 ppm) in a 5-mm coaxial tube, were 0.13, 0.34, and 0.74 M for A_2T_2, 0.16, 0.38, and 0.78 M for A_4T_4, and 0.21, 0.42, and 0.82 M for TA. Crystalline netropsin (>98%), obtained from Boehringer Mannheim, was added directly to the NMR samples, yielding netropsin/duplex mole ratios of 1.0 ± 0.1 for A_2T_2 and 1.1 ± 0.1 for A_4T_4 and TA. In the ion competition experiments, dry KCl, RbCl, CsCl, or NH_4Cl was added directly to the NMR samples.

MRD Experiments. Longitudinal (inversion recovery) and transverse (spin echo) magnetic relaxation measurements were performed at 10 magnetic field strengths by using five NMR spectrometers operating in the field range of 0.2–14.1 T, corresponding to ^{23}Na resonance frequencies in the range of 2.3–159 MHz. Measurements below 1.2 T (13.2 MHz) were performed with an iron magnet equipped with field-variable lock and flux stabilizer (29), whereas the higher fields were accessed by conventional superconducting magnets. In each experiment, 40 spectra were accumulated with the variable relaxation delay spanning the range of 0.05 R_f^{-1}–5.1 R_s^{-1}, where R_f and R_s are the rates of the fast and slow components of the biexponential longitudinal or transverse magnetization recovery or decay. The duration of the 90° pulse was less than 15 μs, and the recycle delay was at least 5 R_s^{-1} in all cases. An acquisition delay of 100–210 μs was used to filter out the solid-like signal from sodium in the NMR tube. To eliminate acoustic ringing at frequencies less than 15 MHz, a composite 90° pulse (30) was used in the inversion-recovery sequence. Pulse amplitude and phase imperfections were compensated by standard phase cycling. To maintain the signal-to-noise ratio above 100 (above 60 at the lowest fields), up to 6×10^4 scans (2×10^5 scans at the lowest fields) were accumulated. All spectra were Fourier-transformed and phase- and baseline-corrected, and the peak was integrated between points where the peak intensity had dropped well below the noise level.

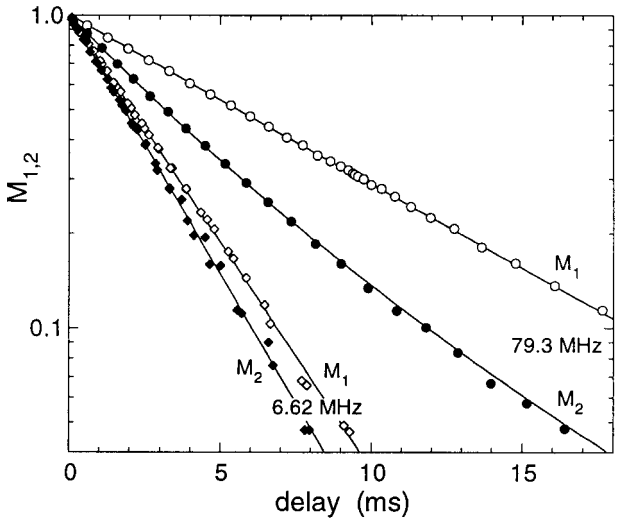

Fig. 1. Relaxation of nonequilibrium longitudinal (open symbols) and transverse (solid symbols) ^{23}Na magnetization after a 180° (inversion recovery) or 90° (spin echo) pulse, respectively, for 8.2 mM A_2T_2 duplex in D_2O (no added salt) at 4°C and pH 7.0. The normalized integrated intensity of the ^{23}Na peak at 6.62 MHz (◇, ◆) and 79.3 MHz (○, ●) is shown. The curves resulted from a global fit of biexponential relaxation functions to the full set of relaxation data taken at nine magnetic fields.

On all spectrometers, the sample temperature was adjusted to 4.00 ± 0.05°C with a copper–constantan thermocouple and was maintained to within ±0.1°C with a thermostated air flow. The volume of the NMR samples in 10-mm tubes was 0.13–0.9 ml.

For reference purposes, the ^{23}Na relaxation rates from a 1-M NaCl solution in D_2O were measured at 4.0°C and at several field strengths, yielding $R_{bulk} = 34.8 \pm 0.3\ s^{-1}$. For the analysis of the ion competition experiments, the ^{23}Na relaxation rate in the absence of DNA was taken to depend on the total salt concentration, m (kg·mol^{-1}), according to $R_{bulk}(m) = R_{bulk}(0)\ (1 + 0.075\ m)$ (31).

Relaxation Data Analysis. Being a spin-3/2 nucleus, ^{23}Na has an intrinsically biexponential relaxation (25). In practice, however, biexponentiality is detectable only in the transverse relaxation above *ca.* 20 MHz (Fig. 1). Transverse relaxation data from frequencies below 20 MHz and longitudinal relaxation data at all frequencies therefore were fitted initially to monoexponential relaxation functions, yielding the effective longitudinal and transverse relaxation rates $R_1^{eff} = 0.2\ R_{1f} + 0.8\ R_{1s}$ and $R_2^{eff} = 0.6\ R_{2f} + 0.4\ R_{2s}$, respectively (25). At higher frequencies, five-parameter fits to a biexponential transverse relaxation function yielded the individual transverse relaxation rates R_{2f} and R_{2s}. In the latter fits, the amplitude ratio for the two exponentials was close to the theoretical value (0.6/0.4 = 1.5) and the offset did not deviate significantly from zero.

To extract a map $J(\nu_i)$ of the spectral density function (SDF) from the relaxation rates, simultaneous fits of 13 or 14 SDF values to the full set of relaxation data at 9 or 10 frequencies were performed. The relaxation rates at each experimental frequency ν_i are related to the SDF values $J(0)$, $J(\nu_i)$, and $J(2\nu_i)$ according to $R_{1f} = J(\nu_i)$, $R_{1s} = J(2\nu_i)$, $R_{2f} = 0.5\ [J(0) + J(\nu_i)]$, and $R_{2s} = 0.5\ [J(\nu_i) + J(2\nu_i)]$, where $J(\nu_i) = (2/5)\ \pi^2\ \chi^2\ J(\nu_i)$ and χ is the quadrupole coupling constant (QCC) (25). Because the frequency list (2.34, 3.31, 4.67, 6.62, 9.34, 13.2, 26.5, 52.9, 79.3, 158.7 MHz) contained seven pairs of frequencies differing by a factor

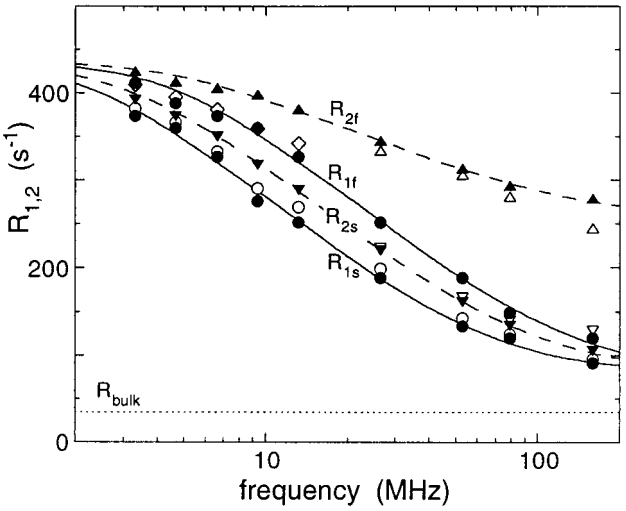

Fig. 2. Result of the global fit of 13 SDF values $J(\nu_i)$ to the ^{23}Na relaxation data from the same sample as in Fig. 1 plotted as fast and slow longitudinal (R_{1f} and R_{1s}, ●) and transverse (R_{2f} and R_{2s}, ▲) relaxation rates. The estimated error bars are of the same size as the data symbols. For comparison, relaxation rates from single-frequency fits are also shown (without error bars) as open symbols: R_1^{eff} (○), R_2^{eff} (◇, at lower fields), and R_{2f} and R_{2s} (△, at higher fields). The curves are based on an assumed form of the SDF.

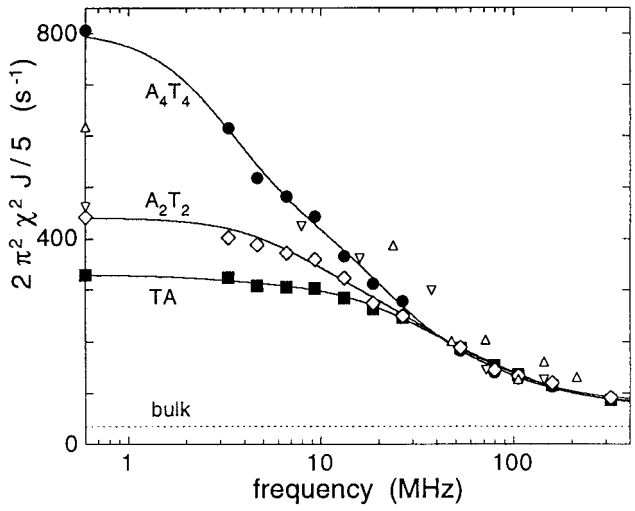

Fig. 3. Map of SDF $J(\nu_i)$ obtained from the global fit to the ^{23}Na relaxation data from aqueous solutions of the dodecamers A_2T_2 (◇), A_4T_4 (●), and TA (■), all at 4°C and pH 7.0 (no added salt). The points on the vertical axis represent SDF values at zero frequency, $J(0)$. The estimated error bars are of the same size as the data symbols. For comparison, literature data (22, 23) for 146-bp nucleosome core DNA at 5°C are also included (▽ and △, respectively).

2.000 ± 0.002, the global fit involved only 14 SDF values, including $J(0)$. An additional 20 parameters were used for overall scaling of the longitudinal and transverse magnetization at the 10 fields. The amplitude ratios of the two exponentials in the longitudinal and transverse relaxation functions were fixed at the theoretical values of 4.0 and 1.5, respectively, and the offset parameters (magnetization at infinite delay time) were set to the values obtained in the initial (single-frequency) fits. Because the signal-to-noise ratio was not the same at all frequencies, the data were weighted in the global fit by the rms deviation obtained from the single-frequency fits. The solid symbols in Fig. 2 are the individual relaxation rates at the experimental frequencies, calculated from the above relations with $J(\nu_i)$ values from the global fit. The overall agreement with the results of single-frequency fits (Fig. 2, open symbols) is good. Whereas the fitted SDF values $J(\nu_i)$ are completely model-independent, the curves in Fig. 2 were obtained by fitting a particular functional form of the SDF (*vide infra*) to the $J(\nu_i)$ values.

Results

General Features of the SDF. Fig. 3 shows a map of the SDF for the three investigated dodecamers. The SDF depends strongly on nucleotide sequence and, in all cases, is distinctly non-Lorentzian. The curves represent fits to a function with three Lorentzian components plus a constant (frequency-independent) contribution. A function with only one or two Lorentzian components (not shown) does not represent the data adequately.

The SDFs of all three dodecamers converge at high (>50-MHz) frequencies, indicating that the highest-frequency Lorentzian component and the constant term are independent of nucleotide sequence. These SDF contributions therefore can be attributed to Na^+ ions that do not interact specifically with the DNA duplex. The frequency-independent contribution to the relaxation rate is 80 ± 2 s^{-1}, larger than for bulk NaCl (35 s^{-1}, see above), as expected because it includes a contribution from subnanosecond electric field gradient fluctuations experienced by the mobile but slightly perturbed Na^+ ions in the diffuse counterion atmosphere surrounding the DNA duplex (25). As expected, the frequency-independent relaxation contribution for all three dodecamers and at the three investigated salt concentrations varies linearly with the fraction "condensed" counterions (data not shown), calculated as 0.76 [P]/$[Na^+]_{tot}$, where [P] is the DNA phosphate concentration (25).

The lowest-frequency Lorentzian component exhibits the strongest sequence dependence and thus reflects those Na^+ ions that are most intimately associated with the DNA. The correlation time of 20–40 ns for this counterion fraction agrees roughly with the DNA tumbling time, estimated to 40 ns in a separate ^{31}P relaxation experiment (32) for A_2T_2 (data not shown). Because the rates of DNA tumbling and counterion exchange (out of a binding site) contribute additively to the observed correlation rate (inverse correlation time), the 20- to 40-ns correlation time can be taken as a lower bound for the mean residence time of these specifically bound Na^+ ions (26). An upper bound is provided by the shortest intrinsic ^{23}Na relaxation time (26), which is about 5 μs for a QCC of 1.3 MHz (see below).

The other two Lorentzian components have correlation times in the range of 1–7 ns. Although these components may not represent distinct physical processes, the time scale is as expected for Na^+ diffusion over the surface of the DNA duplex. This motion modulates the magnitude and orientation of the electric field gradient (motionally averaged by picosecond hydration shell dynamics) as the ion "jumps" across the grooves and diffuses around the helix axis (33, 34).

Evidence for Minor-Groove Binding. To determine the location of the most tightly bound Na^+ ions, we performed a difference MRD experiment, mapping the SDF before and after addition of one equivalent of the minor groove-binding drug netropsin (Fig. 4). Whereas netropsin binding reduces the magnitude of all components in the SDF, the lowest-frequency component decreases most dramatically and is virtually eliminated for A_2T_2. (The dispersion from the A_2T_2–netropsin complex can be modeled adequately by a single Lorentzian component with a correlation time of 1.5 ns.) We conclude that the most tightly bound Na^+ ions reside in the minor groove and are displaced by netropsin. For A_2T_2, netropsin is known to bind in the central AT tract (35, 36), where the minor groove is most strongly narrowed.

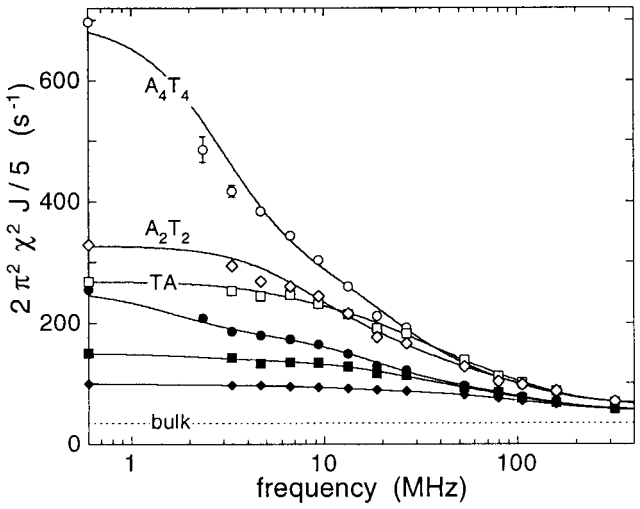

Fig. 4. Same as in Fig. 3, but for samples with 0.34–0.42 M Na^+ before (open symbols) and after (solid symbols) addition of one equivalent netropsin.

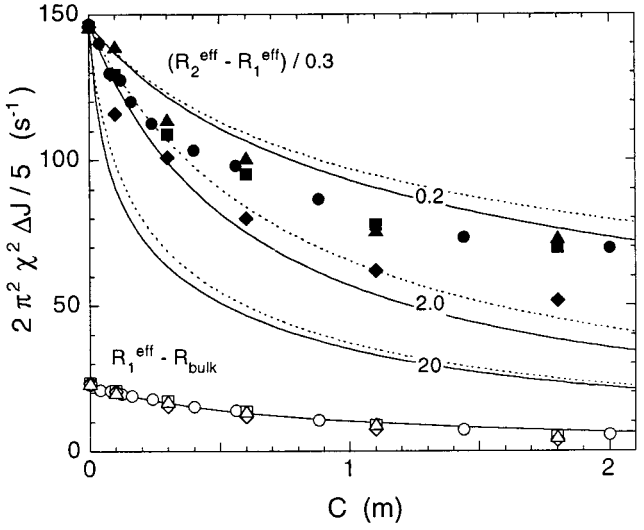

Fig. 5. Frequency-dependent, $J(0) - J_{hf}$ (solid symbols), and frequency-independent, $J_{hf} - J_{bulk}$ (open symbols), SDF components, derived from the effective ^{23}Na relaxation rates R_1^{eff} and R_2^{eff} at 158.7 MHz and 4°C, as functions of added salt: KCl (●, ○), RbCl (□, ■), CsCl (▲, △), and NH_4Cl (◆, ◇). The samples contained 8.2 mM A_2T_2 duplex in D_2O and 0.74 M NaCl. The curves were calculated as described in the text. The curve labels refer to the binding constant K_M (M^{-1}) of the competing ion.

This region therefore must also contain the strongest Na^+-binding site(s). The larger low-frequency component for A_4T_4 (Figs. 3 and 4) and its less complete elimination by netropsin (Fig. 4) are consistent with the longer, narrowed AT tract (nearly twice the length of the netropsin molecule) in this dodecamer. The TA duplex is known to have a uniformly wide minor groove (37), and the relatively small low-frequency component (Figs. 3 and 4) therefore suggests that the affinity of Na^+ binding is reduced by a wide groove. Nevertheless, the observation of a significant low-frequency component also for the TA dodecamer shows that an ApT step is not necessary for long-lived Na^+ binding. The incomplete elimination of the low-frequency component by netropsin (Fig. 4) may reflect a weaker (or asymmetric) binding of the drug to the TA duplex.

Sodium Ion Occupancy. The magnitude β of the low-frequency SDF component is related to the number N_b of long-lived Na^+-binding sites and their mean occupancy θ_b through (25, 26) $\beta = (2/5)\ \pi^2\ \chi^2\ N_b\ \theta_b/N_t$, where N_t is the total number of Na^+ ions per duplex (22 for a dodecamer without added salt). The QCC χ was estimated by computing the electric field gradient tensor at several sites in the minor groove of the A_2T_2 crystal structure, assuming a rigid binding geometry and using the standard nuclear parameters $Q = 0.11$ barn and $1 + \gamma_\infty = 5.1$. Partial charges were taken from the AMBER force field (38) for DNA and from the SPC water model. Hydrogen atoms were merged with the attached heavy atoms, and a cutoff of 4 Å was used (very similar results were obtained for 3 Å or 5 Å). For the five central nominal water sites in the primary spine of hydration of A_2T_2, we thus obtained $\chi = 1.3 \pm 0.2$ MHz, with no significant difference between two crystal structures (5, 7). Although this estimate is crude, it is reassuring to note that QCCs for oxygen-coordinated Na^+ derived from ^{23}Na NMR studies of cryptands (39) and inorganic solids (40) as well as from molecular simulations (41, 42) generally fall in the range of 1–2 MHz.

With a QCC of about 1 MHz, the experimental β values yield $N_b\ \theta_b \ll 1$. Even if we assume a single Na^+ site ($N_b = 1$), we obtain (with $\chi = 1.3$ MHz) occupancies of only a few percent, e.g., $\theta_b = 0.05$ for A_2T_2 and A_4T_4 and $\theta_b = 0.01$ for TA at a Na^+ concentration of about 0.4 M (where the most accurate SDF data were obtained). These low occupancies, corresponding to a binding constant K_{Na} of 0.03 M^{-1} for TA and 0.1 M^{-1} for the other two dodecamers, are consistent with the weak observed salt dependence in β (data not shown). (A quantitative analysis of the effect of added NaCl is complicated by an apparent salt dependence of the correlation times and therefore was not attempted.) We note that if our QCC estimate were in error by a factor of 2, the quoted ion occupancies and binding constants would change by a factor of 4.

Competitive Ion Binding. The relative affinities of different monovalent counterions for the specific binding site(s) in the minor groove of A_2T_2 were assessed by measuring R_1^{eff} and R_2^{eff} for ^{23}Na at 159 MHz as KCl, RbCl, CsCl, or NH_4Cl was added to A_2T_2 solutions containing excess NaCl (0.74 M Na^+). Fig. 5 shows the salt dependence of $(R_2^{eff} - R_1^{eff})/0.3 = J(0) - J_{hf}$ and $R_1^{eff} - R_{bulk} = J_{hf} - J_{bulk}$, where J_{hf} is the value of the SDF on the high-frequency plateau (Fig. 3). The former quantity is dominated (≥50%) by the slowest (sequence-specific) Lorentzian component. The frequency-independent contribution $J_{hf} - J_{bulk}$ scales as $1/(1 + [M^+]_{tot}/[Na^+]_{tot})$ for all investigated salts (bottom curve in Fig. 5), as expected for nonlocalized counterion association (25, 43). In contrast, $J(0) - J_{hf}$ exhibits a stronger salt dependence in all cases. The set of associated curves in Fig. 5 were calculated by assuming a 50% nonspecific contribution (the fast and intermediate Lorentzian components) scaling as $J_{hf} - J_{bulk}$ and a 50% site-binding contribution (the slowest, strongly sequence-specific, Lorentzian component) scaling as $1/[1 + K_M\ [M^+]_{tot}/(1 + K_{Na}\ [Na^+]_{tot})]$, as expected for weak site binding ($[M^+]_{bound} \ll [M^+]_{free}$). The three pairs of curves pertain to a binding constant K_M for the competing ion of 0.2, 2.0, and 20 M^{-1}, with $K_{Na} = 0.1\ M^{-1}$ (solid curves) or 1 M^{-1} (dashed curves). The results in Fig. 5 indicate that K^+, Rb^+, and Cs^+ all bind with similar or slightly higher affinity than Na^+, whereas NH_4^+ binding is considerably stronger (by an order of magnitude if $K_{Na} = 0.1\ M^{-1}$). These findings agree qualitatively with results from previous ^{23}Na NMR studies of competitive counterion binding to polymeric DNA (43).

Discussion

Fig. 3 includes previously reported SDF values derived from field-dependent ^{23}Na relaxation in solutions of 146-bp restriction fragments of nucleosome core DNA (22, 23). Because the

tumbling time of these fragments is three orders of magnitude longer than for a dodecamer, the near agreement with our results implies that the residence time of groove-bound Na^+ ions is not much longer than the correlation time (20–40 ns) of the lowest-frequency Lorentzian component obtained here (see above). The low occupancy implies that Na^+ binding in the minor groove is a rare event: on average, the site is occupied by a sodium ion for some 50 ns and then is visited by some 1,000 water molecules, each one residing, on average, 1 ns (27) before another ion enters the site. Such infrequent intrusions of Na^+ into the minor groove are not likely to be detected in a 5-ns MD trajectory, nor would such low occupancies be detectable by x-ray diffraction. Although we do find evidence of Na^+ binding in the minor groove, with an occupancy of only a few percent, groove-bound ions are not likely to contribute importantly to the ensemble of DNA structures present under physiological conditions. In particular, groove-bound Na^+ ions do not appear to play a major role in AT-tract bending or groove narrowing (5, 6, 13, 14).

The low Na^+ occupancy (a few percent) in minor-groove sites and the similarly weak specific binding affinity of the other alkali metal ions inferred from the present data at 277 K are not necessarily inconsistent with a higher occupancy at the cryogenic temperatures (120–160 K) used in recent crystallographic studies. Even a modest binding enthalpy of 5 $kJ \cdot mol^{-1}$ could increase the binding constant from 0.1 M^{-1} at 277 K to 1.7 M^{-1} at 120 K, which is sufficient to give 50% occupancy in a single binding site, as found for Rb^+ at the ApT step in A_2T_2 (11). On the other hand, our competition data (Fig. 5) indicate a NH_4^+-binding constant of less than 2 M^{-1}, whereas a much larger binding constant (20–30 M^{-1}) would be required to achieve, for example, 10% NH_4^+ occupancy of a single site in the absence of competing ions. In the NOESY study, NH_4^+ binding was indicated by cross-peaks with the H2 protons of all four or five adenines in three different *B*-DNA duplexes in the presence of a 10- to 15-fold excess of Na^+ or Li^+ ions (18). It seems unlikely that the NOESY method could detect an ion occupancy of much lower than 10%.

Sodium ion binding in the minor groove also can be studied via the quadrupolar splitting of the ^{23}Na resonance in a macroscopically aligned DNA sample. A single Na^+ site per 12 bp with an occupancy of 5% and a QCC of 1.3 MHz could produce a splitting as large as 1,500 Hz, depending on the orientation of the electric field gradient relative to the magnetic field (33, 34). Reported ^{23}Na splittings from the cholesteric liquid-crystalline phase of *ca.* 150-bp nucleosome core DNA from chicken erythrocyte (23) and calf thymus (44) do not exceed 800 Hz, but this can be attributed to partial cancellation of splitting contributions from Na^+ sites with differently oriented electric field gradients. The strong observed temperature dependence of the splitting (23) and its zero-crossing on temperature variation (44) indicate a dominant contribution from site-bound Na^+ ions (presumably in the minor groove) rather than from the diffuse ion atmosphere. Further quadrupolar splitting studies with DNA fragments of known sequence and in the presence of competing species thus may be rewarding.

This work was supported by grants from the Crafoord Foundation and the Swedish Natural Science Research Council (NFR). We are grateful to the editor for bringing ref. 8 to our attention.

1. Mirzabekov, A. D. & Rich, A. (1979) *Proc. Natl. Acad. Sci. USA* **76,** 1118–1121.
2. Rouzina, I. & Bloomfield, V. A. (1999) *Biophys. J.* **74,** 3152–3164.
3. Seeman, N. C., Rosenberg, J. M., Suddath, F. L., Kim, J. J. P. & Rich, A. (1976) *J. Mol. Biol.* **104,** 109–144.
4. Chandrasekaran, R., Radha, A. & Park, H.-S. (1995) *Acta Cryst. D* **51,** 1025–1035.
5. Shui, X., McFail-Isom, L., Hu, G. G. & Williams, L. D. (1998) *Biochemistry* **37,** 8341–8355.
6. McFail-Isom, L., Sines, C. S. & Williams, L. D. (1999) *Curr. Opin. Struct. Biol.* **9,** 298–304.
7. Tereshko, V., Minasov, G. & Egli, M. (1999) *J. Am. Chem. Soc.* **121,** 470–471.
8. Chiu, T. K., Kaczor-Grzeskowiak, M. & Dickerson, R. E. (1999) *J. Mol. Biol.* **292,** 589–608.
9. Drew, H. R. & Dickerson, R. E. (1981) *J. Mol. Biol.* **151,** 535–556.
10. Shui, X., Sines, C. C., McFail-Isom, L., VanDerveer, D. & Williams, L. D. (1998) *Biochemistry* **37,** 16877–16887.
11. Tereshko, V., Minasov, G. & Egli, M. (1999) *J. Am. Chem. Soc.* **121,** 3590–3595.
12. Bartenev, V. N., Golovamov, Eu, I., Kapitonova, K. A., Mokulskii, M. A., Volkova, L. I. & Skuratovskii, I. Y. (1983) *J. Mol. Biol.* **169,** 217–234.
13. Young, M. A., Jayaram, B. & Beveridge, D. L. (1997) *J. Am. Chem. Soc.* **119,** 59–69.
14. Young, M. A., Ravishanker, G. & Beveridge, D. L. (1997) *Biophys. J.* **73,** 2313–2336.
15. Lavery, R. & Pullman, B. (1985) *J. Biomol. Struct. Dyn.* **5,** 1021–1032.
16. Feig, M. & Pettitt, B. M. (1999) *J. Mol. Biol.* **286,** 1075–1095.
17. Auffinger, P. & Westhof, E. (1998) *Curr. Opin. Struct. Biol.* **8,** 227–236.
18. Hud, N. V., Sklenár, V. & Feigon, J. (1999) *J. Mol. Biol.* **286,** 651–660.
19. Hud, N. V. & Feigon, J. (1997) *J. Am. Chem. Soc.* **119,** 5756–5757.
20. Reuben, J., Shporer, M. & Gabbay, E. J. (1975) *Proc. Natl. Acad. Sci. USA* **72,** 245–247.
21. Nordenskiöld, L., Chang, D. K., Anderson, C. F. & Record, M. T. (1984) *Biochemistry* **23,** 4309–4317.
22. van Dijk, L., Gruwel, M. L. H., Jesse, W., de Bleijser, J. & Leyte, J. C. (1987) *Biopolymers* **26,** 261–284.
23. Groot, L. C. A., van der Maarel, J. R. C. & Leyte, J. C. (1994) *J. Phys. Chem.* **98,** 2699–2705.
24. Stein, V. M., Bond, J. P., Capp, M. W., Anderson, C. F. & Record, M. T. (1995) *Biophys. J.* **68,** 1063–1072.
25. Braunlin, W. H. (1995) in *Adv. Biophys. Chem.*, ed. Bush, C. A. (JAI Press, Greenwich, CT), Vol. 5, pp. 89–139.
26. Halle, B., Denisov, V. P. & Venu, K. (1999) in *Biological Magnetic Resonance*, eds. Krishna, N. R. & Berliner, L. J. (Kluwer/Plenum, New York), Vol. 17, pp. 419–484.
27. Denisov, V. P., Carlström, G., Venu, K. & Halle, B. (1997) *J. Mol. Biol.* **268,** 118–136.
28. Jóhannesson, H. & Halle, B. (1998) *J. Am. Chem. Soc.* **120,** 6859–6870.
29. Furó, I. & Halle, B. (1995) *Phys. Rev. E* **51,** 466–477.
30. Zhang, S., Wu, X. & Mehring, M. (1990) *Chem. Phys. Lett.* **173,** 481–484.
31. Hertz, H. G., Holz, M., Keller, G., Versmold, H. & Yoon, C. (1974) *Ber. Bunsenges. Phys. Chem.* **78,** 493–509.
32. Lane, A. N. (1995) *Methods Enzymol.* **261,** 413–435.
33. Quist, P.-O., Halle, B. & Furó, I. (1991) *J. Chem. Phys.* **95,** 6945–6961.
34. Schultz, J., Andreasson, B., Nordenskiöld, L. & Rupprecht, A. (1994) *J. Phys. Chem.* **98,** 8507–8518.
35. Patel, D. J. (1982) *Proc. Natl. Acad. Sci. USA* **79,** 6424–6428.
36. Goodsell, D. S., Kopka, M. L. & Dickerson, R. E. (1995) *Biochemistry* **34,** 4983–4993.
37. Urpi, L., Tereshko, V., Malinina, L., Huynh-Dinh, T. & Subirana, J. A. (1996) *Nat. Struct. Biol.* **3,** 325–328.
38. Cornell, W. D., Cieplak, P., Bayly, C. I., Gould, I. R., Merz, K. M., Ferguson, D. M., Spellmeyer, D. C., Fox, T., Caldwell, J. W. & Kollman, P. A. (1995) *J. Am. Chem. Soc.* **117,** 5179–5197.
39. van der Maarel, J. R. C., van Duijn, D., de Bleijser, J. & Leyte, J. C. (1987) *Chem. Phys. Lett.* **135,** 62–66.
40. Koller, H., Engelhardt, G., Kentgens, A. P. M. & Sauer, J. (1994) *J. Phys. Chem.* **98,** 1544–1551.
41. Linse, P. & Halle, B. (1989) *Mol. Phys.* **67,** 537–573.
42. Chen, S. W. & Rossky, P. J. (1993) *J. Phys. Chem.* **97,** 10803–10812.
43. Bleam, M. L., Anderson, C. F. & Record, M. T. (1980) *Proc. Natl. Acad. Sci. USA* **77,** 3085–3089.
44. Strzelecka, T. E. & Rill, R. L. (1990) *Biopolymers* **30,** 803–814.